Remote Sensing of Environment 166 (2015) 154–162

Contents lists available at ScienceDirect

Remote Sensing of Environment

journal homepage: www.elsevier.com/locate/rse

Impact of Sahara dust on solar radiation at Cape Verde Islands derived from MODIS and surface measurements

Swati Gehlot [a,*], Peter J. Minnett [b], Detlef Stammer [a]

[a] Center für Erdsystemwissenschaften und Nachhaltigkeit, University of Hamburg, Bundesstrasse 53, Hamburg, 20146, Germany
[b] Rosenstiel School of Marine and Atmospheric Science, University of Miami, 4600 Rickenbacker Causeway, Miami, FL 33149-1098, USA

ARTICLE INFO

Article history:
Received 3 December 2014
Received in revised form 19 May 2015
Accepted 29 May 2015
Available online 24 June 2015

Keywords:
Sahara dust
Radiation
MODIS
Aeronet
AOD

ABSTRACT

Based on radiometer measurements of solar irradiance (direct and diffuse light) and Aeronet-based aerosol optical depth (AOD) obtained at the Cape Verde atmospheric observatory during a major cloud-free dust outbreak event on February 7, 2012, the relationship between Saharan mineral dust outbreaks and a reduction of solar irradiance is quantified. The investigation is representative of the eastern subtropical North Atlantic region where the wind mobilization of mineral desert dust from the Sahara results in aerosol signals that are large enough to outweigh those from other aerosol types such as anthropogenic and marine aerosols. Ground-based estimates of AOD show frequency dependence as is expected from Mie theory. Our AOD signals agree well with satellite-based MODIS products and reveal AOD values exceeding 2.5 during the investigated dust storm event. We also demonstrate the use of satellite imagery with an atmospheric trajectory model to simulate time series of measurements at a given location. Using this approach, variations in AOD observed during February 7, 2012 can be rationalized as spatial inhomogeneities in the atmospheric dust load being advected laterally over the observing site. Our measurements suggest a dust forcing efficiency of around -90 W/m^2/AOD at a wavelength of 380 nm, which is about 10–15% greater than reported in the literature indicative of a possible non-linear behavior at high AODs.

1. Introduction

The radiation budget of the Earth's atmosphere is greatly influenced by the amount and type of atmospheric aerosols (Kaufman, Tanre, & Boucher, 2002). Atmospheric aerosols modify the incoming and outgoing radiation (Tegen et al., 1997) directly through scattering and absorption and indirectly by impacting cloud formation processes, and subsequently the precipitation characteristics (Albrecht, 1989; Kaufman et al., 2002; Rosenfeld, Rudich, & Lahav, 2001; Sokolik et al., 2001; Twomey, 1977). For the sign and magnitude of the mineral dust radiative forcing, however, the most important factor for the shortwave radiative forcing is the single scattering albedo (related to atmospheric opacity) whereas the longwave radiative forcing is dependent on the vertical profile of the dust concentrations (Forster et al., 2007; Vogelmann, Flatau, Szczodrak, Markowicz, & Minnett, 2003). In addition to the dust types/size(s) and the geographical location, their complex mineral composition leads to highly uncertain effects on dust-related radiative forcing. Despite of being a core element of radiation and climate forcing, the knowledge of dust–radiation–climate impacts are still rudimentary (Chiapello, Moulin, & Prospero, 2005; Forster et al., 2007; Prospero, 1999; Prospero & Carlson, 1972). According to the Intergovernmental Panel on Climate Change (IPCC) AR5 report, the radiative forcing from aerosol–radiation interactions contribute to a major part of the largest uncertainty in quantifying the earth's radiation budget (IPCC AR5, 2013).

The Saharan region is a major source of mineral dust aerosols for the Atlantic atmosphere. After being advected across the North Atlantic Ocean (Kaufman et al., 2005) via large scale atmospheric circulation those mineral dust particles are a prime aerosol constituent of the lower atmosphere downwind of the Saharan region. As a consequence, they have a substantial influence on the solar and infrared radiation budget at sea level over the eastern subtropical North Atlantic (Evan, Foltz, Zhang, & Vimont, 2011; Lau & Kim, 2007). Studying the interaction of Sahara mineral dust with solar incoming shortwave radiation provides an important opportunity to determine its climate forcing efficiencies. Related previous studies showed multiple instances of enhanced dust concentration over the west African coast that led to a relative cooling of the ocean surface by scattering of solar radiation (Lau & Kim, 2007; Li, Vogelmann, & Ramanathan, 2004; Zhu, Ramanathan, Li, & Kim, 2007). Although many model and satellite based studies have been performed showing the absorption of solar radiation by dust (Chin et al., 2002; Evan et al., 2011; Kaufman, Tanre, Dubovik, Karnieli, & Remer, 2001; Kaufman et al., 2002; Li et al.,

* Corresponding author.
E-mail address: swati.gehlot@zmaw.de (S. Gehlot).

http://dx.doi.org/10.1016/j.rse.2015.05.026

2004), ground-based radiation measurements are still the basic method for the validation of the surface aerosol radiative forcing estimates (Holben et al., 2001).

Using a synthesis of recently obtained ground based observations of radiation and aerosol optical thickness estimates at the Cape Verde Islands, the present study revisits the question of the impact of Saharan dust on the solar incoming radiative forcing in the eastern subtropical Atlantic Ocean. In detail, we investigate the dust aerosol optical properties in a cloud-free atmosphere during a Saharan dust outbreak and quantify the dust forcing efficiency. In addition, we use the ground based results to test MODIS (moderate resolution imaging spectroradiometer) retrievals of the atmospheric aerosol optical thickness. The volcanic archipelago of Cape Verde Islands, located about 600 km west of Senegal, is specifically suited for these studies since these islands are located within the primary dust transport area over the tropical Atlantic (Chiapello et al., 1997; Schütz, 1980) and because the dust load over this area is therefore relatively abundant in comparison to the non-sea salt sulfate aerosols leading it to be the dominant light scattering aerosol for this region (Li, Mating, Savoie, Voss, & Prospero, 1996).

2. Radiation measurements at Cape Verde Islands

All in situ measurements analyzed here were taken at the Cape Verde Atmospheric Observatory *Humberto Duarte Fonseca* located at Calhau on a northwest facing sandy beach on São Vicente at 24.9°W–16.8°N, adjacent to the ocean, with the prevailing trade winds blowing directly off the ocean (Fig. 1a). Our instrumentation consists of two stand-alone highly integrated ultraviolet (UV)–visible (VIS) hyper-spectral radiometers (RAMSES–ACC–VIS hyper-spectral radiometer manufactured by TriOS) and an automatic sun photometer CIMEL CE-318 (Fig. 1b). The sensors measure radiance in the UV–VIS spectral range and irradiance in the UV–VIS and UVA/UVB spectral ranges. Direct solar radiance is radiation that comes from the sun, without scattering or reflection by clouds, atmospheric dust, the ground or other objects. In contrast, irradiance includes diffuse light that is scattered sunlight. The radiometers measure direct radiance and hemispheric irradiance spectra every 5 min starting from 06:00 UTC to 22:00 UTC (producing about 192 spectra per day). The measurement wavelength range is 320 to 950 nm with a spectral resolution of 3.3 nm and a wavelength uncertainty of 0.3 nm. The presently available data are from March 29, 2008 to January 31, 2010, and from March 10, 2011 to present.

Through this project, the automatic sun photometer CIMEL CE-318 deployed at the Cape Verde atmospheric observatory at Calhau, became part of the aerosol robotic network (Aeronet), starting in February 2012. The photometer measures the direct sun radiances in eight channels within the spectral range of 340–1640 nm and sky radiances in four spectral channels (Holben et al., 2001). The ground observations of the raw sun-photometer are processed and stored at the Aeronet archive (http://aeronet.gsfc.nasa.gov/). The spectral channels of 380 nm and 870 nm are used in this study, with AOD level 1.5 data (cloud-screened and quality checked as detailed in Smirnov, Holben, Eck, Dubovik, and Slutsker (2000)) from the Aeronet archive for the Calhau site.

Aerosol optical depth (AOD) is calculated from spectral extinction of direct beam radiation at each wavelength based on the Beer–Bouguer Law. AOD time series provide a measure of Saharan mineral dust concentrations and can be used to compute the anomaly of solar shortwave irradiance at sea level underneath the dust layer (Li et al., 2004; Martínez Avellaneda, Serra, Minnett, & Stammer, 2010; Yoon, Won, Omar, Kim, & Sohn, 2005). Typically, the uncertainty in AOD estimates derived from a newly calibrated field instrument is smaller than 0.02 under cloud-free conditions. Along with the AOD data provided at every 15 min for the sunlit time of the day, single scattering albedo, and refractive indices of the aerosols are computed via Aeronet inversion algorithm (Dubovik & King, 2000). The Ångström exponent is computed from AOD at the available wavelengths by Aeronet (Holben et al., 1998).

3. Results

3.1. Radiation measurements

Time series of integrated shortwave (SW) radiation computed at top of atmosphere (Q_{TOA}, shown in blue) and measured at sea level (Q_{SL}, shown in red) in the visible spectrum are shown in Fig. 2a for the dust outbreak period of 5 days in Feb 2012. The values of Q_{TOA} were calculated for the position of the sun at the site location and local measurement times using the equations given in the Astronomical Almanac (Astronomical Applications Department, 1990) with the

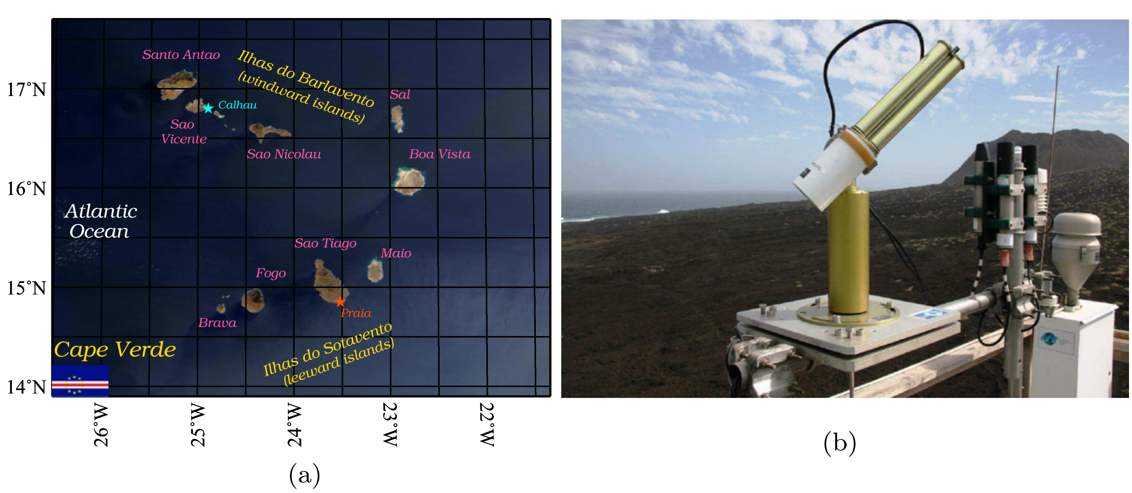

Fig. 1. (a) Map of the Cape Verde archipelago in the eastern subtropical North Atlantic showing the locations of individual islands. The blue star shows the location of the Cape Verde atmospheric Observatory Humberto Duarte Fonseca in São Vicente. (b) The Cape Verde atmospheric observatory tower platform with the instrumentation that consists of a CIMEL sun-photometer measuring AOD at multiple wavelengths (340–1640 nm) together with other columnar optically effective aerosol properties and hyperspectral radiometers measuring solar irradiance in visible and UV spectrum. Also visible are the RAMSES–ACC–VIS hyperspectral radiometers.

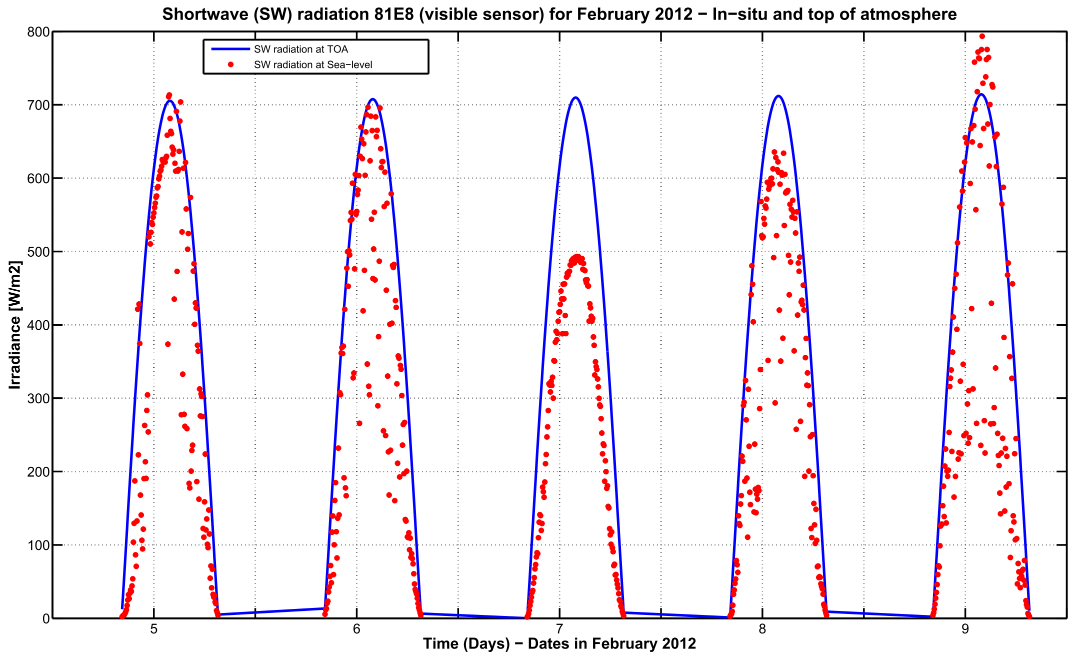

(a)

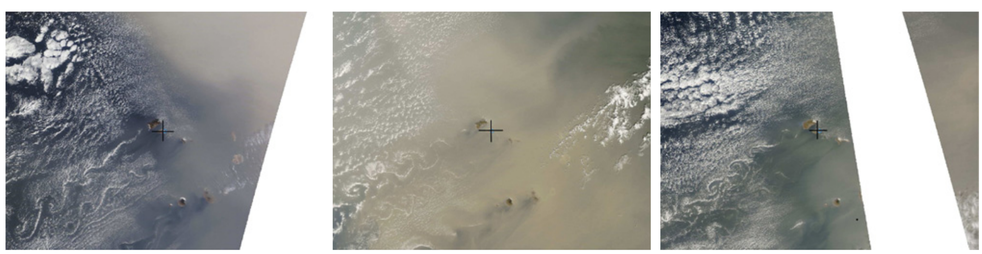

(b) (c) (d)

Fig. 2. (a) Time series of integrated SW radiation computed at top of atmosphere (blue lines) and measured over 5 minute intervals at sea level (red dots) in the visible spectrum for the dust outbreak period of 5 days in Feb 2012. Outliers from the mean daily cycles of measured SW radiation represent the impact of clouds and dust on irradiance profiles due to reflection/scattering. (Bottom row) MODIS Rapid Response System near-real time quasi-true color images of the Cape Verde ground station from February 6 — day with broken clouds (b), February 7 — cloud-free dust outbreak event (c), and February 8 — day with broken clouds (d).

spectral distribution being taken from Thuillier et al. (2003). Values at sea level were obtained by integrating the spectral radiation measurements available every 5 min over the visible wavelength band according to

$$\int_{\lambda_1}^{\lambda_2} f(\lambda) d\lambda, \quad (1)$$

where $\lambda_1 = 400$ nm, $\lambda_2 = 700$ nm and $f(\lambda)$ is the spectral response function of the radiometer. A value of solar irradiance (in Watt/m^2) is obtained every 5 min.

As is obvious from the figure, a major obstacle in studying the influence of Sahara mineral dust on surface radiative budget is the presence of clouds which typically attenuate the downward solar irradiance, depending on the type of clouds and their optical properties. In addition to the spectral attenuation, some cloud instances (for e.g. broken clouds and optically thin clouds) can also increase the surface irradiance by increasing the diffuse sky radiation by scattering (Kirk, 1994; Pfister et al., 2003). Moreover, the presence of cloud leads to significant variability in the AOD observations (Martínez Avellaneda et al., 2010). These effects can be identified in the surface radiation measurements shown in Fig. 2a. What are required for our study are strong dust events under cloud-free conditions, but these are relatively rare.

Selected for this study was a period of 5 days which contained a dust outbreak event that specifically had a cloud-free day resulting in a clear uninterrupted aerosol signal in the sun photometer measurements. The presence of broken clouds during the 5 day observational period can be identified visually in the panels shown in the bottom row of Fig. 2, derived from the MODIS rapid response system near-real time pseudo-true color images of the area around the Cape Verde station from February 6 — a day with broken clouds (Fig. 2b), February 7 — a cloud-free dust event (Fig. 2c), and February 8 — a day with broken clouds (Fig. 2d). Although the MODIS rapid response system near-real-time true color images represent conditions in the region only at the time of the satellite overpass, they reasonably illustrate the presence or absence of clouds over the area of interest. The absence of clouds during February 7, 2012 is apparent in the MODIS image, as is the high dust load during this particular day.

A comparison of the various panels of the figure reveals nicely that the elevated variability from the mean daily cycles represent the impact of clouds and dust on irradiance profiles due to scattering. When the irradiance profile at sea level is as smooth as that at the top of the atmosphere, the influence of clouds can be assumed to be minimal. The time series of measured SW radiation at sea level for February 7, 2012 shows no significant influence on the measurements during this day, and hence the quantitative difference between the top-of-atmosphere and surface short-wave radiation can be attributed to the effect of dust.

3.2. Temporal AOD variations

Based on the data shown in Fig. 2, February 7, 2012, can be identified as a prime — almost perfect — example of a cloud-free dust outbreak event suitable for analysis. This is confirmed by Fig. 3a, showing the AOD over the Calhau site for a few days of February 2012. The figure reveals a substantially increased AOD, up to 2.7, during February 7, 2012, related to a high atmospheric dust load event during that day, a level that is much higher than what can be seen during other days, during which the AOD < 1.0, and <0.5 on many days. Different colors in the figure represent the different spectral channels used in the Aeronet AOD computation and document that the 340 nm channel leads to systematically higher values.

A comparison with daily AOD values at 550 nm provided by the MODIS level 3 (L3 data, quality flagged, 1° × 1°) gridded daily global data product (Acker & Leptoukh, 2007), containing data from MODIS on both Terra and the Aqua satellites and shown as a black line in the figure, reveals a good agreement between the in situ and satellite measurements over the measurement site. A systematic agreement between daily average Aeronet AOD at 500 nm and daily average gridded MODIS L3 AOD at 550 nm (Chan, 2009; Nisantzi, Hadjimitsis, & Alexakis, 2011) can also be inferred from the scatter plot of both parameters, shown in Fig. 3b. In the figure, a significant correlation between the MODIS and the in situ observations is found within the spectral range of 500–550 nm for variable values of aerosol optical depth. The slope of the best-fit straight line to the data points comes out to be 0.995, with norm of residual close to 0.750 showing 75% confidence level.

Expanding the ground-based data from the high dust event of February 7, 2012, in time reveals temporal variations of in situ AOD during that day (Fig. 4). As can be seen from the figure, the dust derived AOD is observed to increase from ~1.5 at 11:00 h to a peak around value of ~2.7 at 13:30 h before subsiding to lower values in the late afternoon.

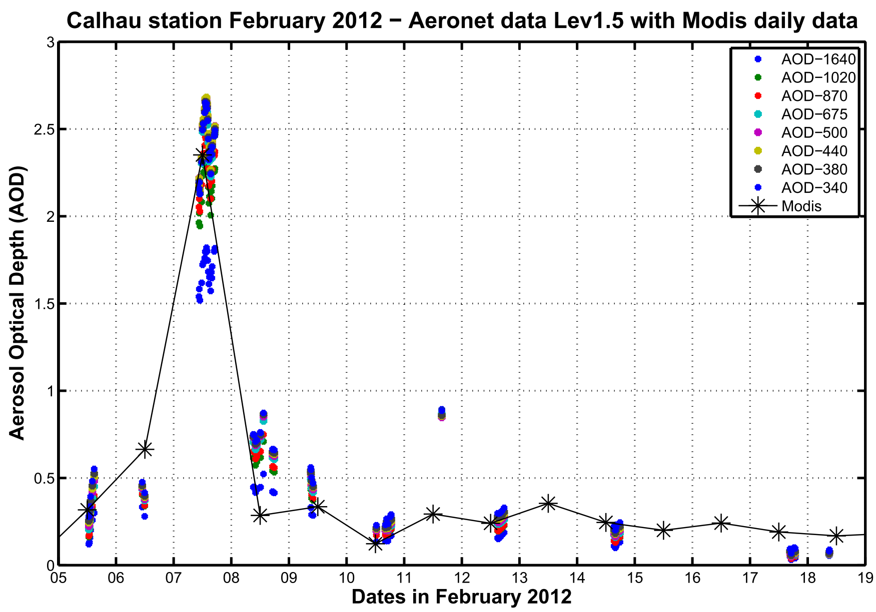

(a)

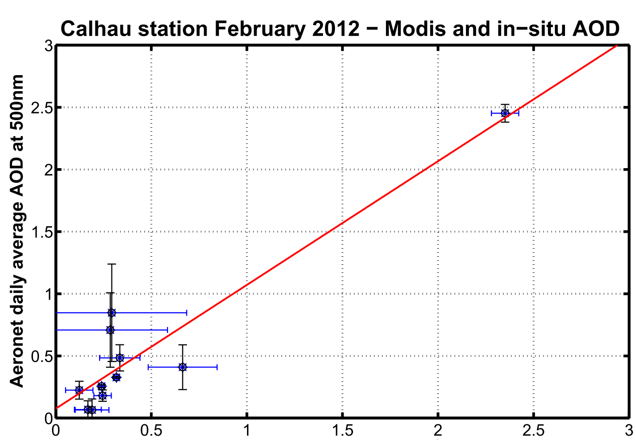

(b)

Fig. 3. (a) Time series of daily in situ AOD at the radiometer location, for the period of 5–19 February, 2012. The variation of AOD is especially high on February 07. Colors represent the different spectral channels used in the Aeronet AOD computation. The daily averaged values of satellite-derived AOD (MODIS level 3 product, AOD at 550 nm) are shown in black asterisks joined by straight lines. (b) Scatter plot of daily averaged values of MODIS gridded AOD measured at 550 nm and Aeronet AOD observations measured at 500 nm.

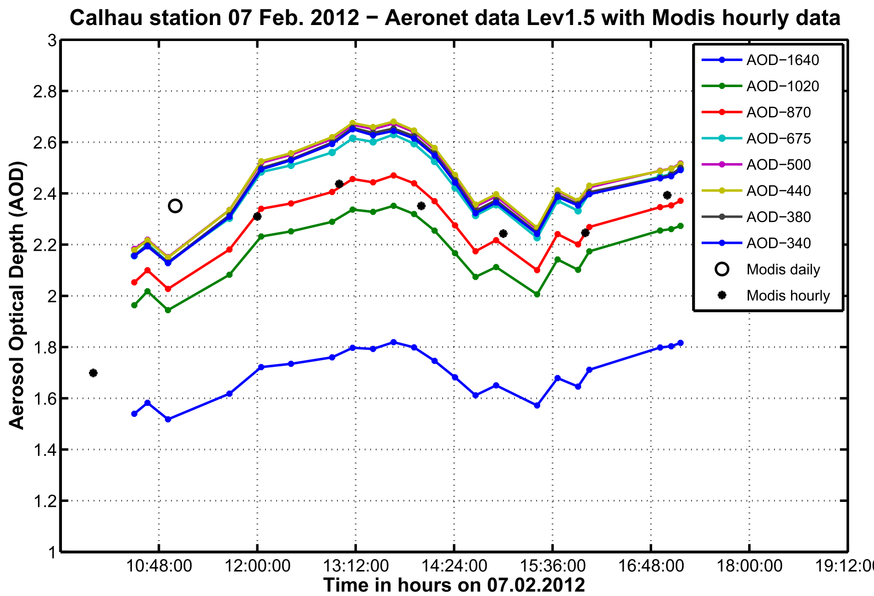

Fig. 4. Time variation of in situ AOD at the radiometer location, for the dust storm event on February 7, 2012. The colors represent the different spectral channels for radiance measurements in Aeronet AOD computation as shown in the inset. For comparison, the daily average MODIS AOD at 550 nm is shown with a black circle (AOD = 2.351 at approximately 11:00 h local time for Terra pass). The MODIS *hourly* values shown in black asterisks represent the simulated variation of MODIS AOD values at the ground observation site based on the movement of dust event via HYSPLIT backward- and forward-trajectory.

Diurnal changes with maxima in the afternoon have been identified in aerosol optical depth measurements elsewhere, but these are mostly seen in terrestrial locations, or downwind of industrial or urban centers, whereas at locations in the open North Atlantic Ocean, diurnal variations are small (Smirnov et al., 2002). Dry deposition of dust over the ocean (Chen & Siefert, 2004; Prospero, 1996) would not lead to an increase in the AOD as seen in the morning. It is therefore most likely that the diurnal signal in the AOD in the ground-based measurements is caused by the advection of spatial variations in the distribution of the dust.

To demonstrate that such sub-daily variations in AOD at a specific location can indeed result from lateral advection of spatial inhomogeneities, we simulate temporal variation of the in situ AOD at our test site during February 7, 2012, by advecting a spatial AOD pattern laterally over our observatory location as it was observed by the MODIS Terra overpass at ~1200 UTC (~1100 local time) during that day. The advection trajectory was determined using the hybrid single-particle Lagrangian integrated trajectory (HYSPLIT) model (Draxler & Rolph, 2013) online tool with NCEP global data assimilation system (GDAS) model winds. From a nearby pass of CALIPSO (cloud-aerosol lidar and infrared pathfinder satellite observations) (Winker, Pelon, & McCormick, 2002) we inferred that the main dust aerosol concentration was at a height of about 1000 m above sea level; hence, the trajectory was calculated at that height.

As a first step, a HYSPLIT back-trajectory was initiated at the observation site 24 h before the dust event reaches the site. A HYSPLIT forward trajectory was conducted subsequently to observe the dust air parcel behavior while it passed the observation site. Considering the trajectory movement in backward and forward directions, the values of AOD at 550 nm from MODIS Terra L2 data (10 km spatial resolution) are extracted to represent temporal variations of AOD at one-hourly intervals at the measurement site. These additional AOD values, derived from MODIS for the dust event on February 7, 2012, are compared in Fig. 4 with the in situ values of AOD. As can be seen, using a purely horizontal movement of the MODIS AOD retrievals along this trajectory, the *hourly* temporal variations at our test site show good agreement with the in situ Aeronet observations suggesting that the horizontal advection of spatial inhomogeneities of atmospheric components can explain temporal variations at a point. The details of the computed trajectories (time, latitude, longitude) and their corresponding values of extracted MODIS AOD are listed in Table 1.

3.3. Dust forcing efficiency

A dust forcing efficiency, f_e (in W/m^2/AOD), can be derived from the available data using the difference between spectrally integrated and daily averaged shortwave radiation at sea level and at the top of the atmosphere as a function of in situ aerosol optical depth. f_e is defined as the rate of change of radiative forcing per unit increase in dust AOD (Ramanathan et al., 2001) according to:

$$f_e = (Q_{SL} - Q_{TOA})/\mathrm{AOD}. \tag{2}$$

Table 1
MODIS derived AOD at 550 nm for both ocean (best) and land (corrected) during 07-02-2012 with best quality data (Quality flag = 3, MODIS) at exact location of site (24.9°W, 16.8°N). The hourly variation of MODIS data is computed using backward- and forward-trajectories via hybrid single-particle Lagrangian integrated trajectory (HYSPLIT) model. The height level is taken to be 1000 m, based on CALIPSO measurements, and the dust event is considered to be moving horizontally neglecting any movement of the trajectory air parcel in the vertical. Considering the trajectory movement in backward and forward directions, the values of AOD at 550 nm from MODIS Terra L2 data (10 km spatial resolution) are extracted to represent a one-hourly temporal variation of AOD at the measurement site. The MODIS Terra pass was at ~1200 UTC (~1100 local time) for the measurement site. The computed values are used in Fig. 4 for details of dust event on 07-02-2012.

Local time on site	Location	MODIS AOD hourly computed
06:00	26.501°W, 16.882°N	2.004
07:00	26.164°W, 16.857°N	2.101
08:00	25.831°W, 16.828°N	1.973
09:00	25.509°W, 16.810°N	1.598
10:00	25.201°W, 16.801°N	1.699
11:00	24.900°W, 16.800°N	–
12:00	24.600°W, 16.810°N	2.310
13:00	24.302°W, 16.831°N	2.437
14:00	24.007°W, 16.855°N	2.351
15:00	23.722°W, 16.883°N	2.243
16:00	23.449°W, 16.978°N	2.246
17:00	23.188°W, 17.040°N	2.393

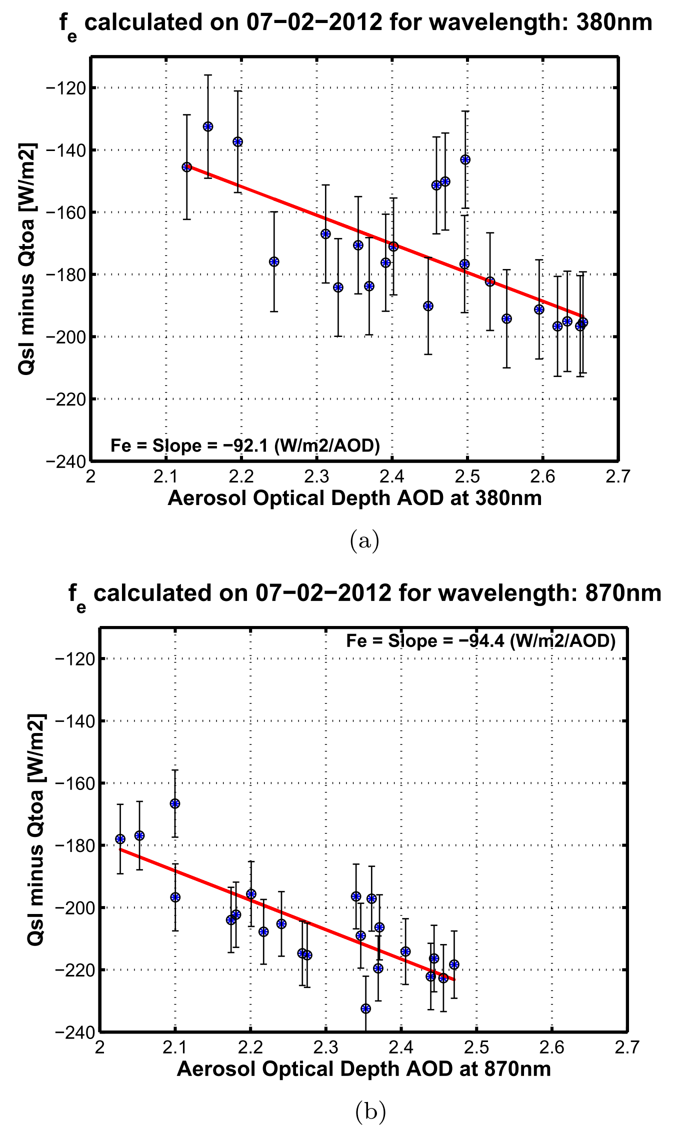

Fig. 5. Dust forcing efficiency calculated for a cloud-free dust event (February 7, 2012) as a function of AOD for (a) at 380 nm, and (b) at 870 nm. Difference between integrated short-wave radiation at sea level and at top of atmosphere as a function of in situ aerosol optical depth measured. The slope of a linear fit represents the value of f_e in W/m^2/AOD.

Here, Q_{SL} and Q_{TOA} are the shortwave radiation fluxes (at a given wavelength) at sea level and at the top of atmosphere respectively. Accordingly, f_e can be derived from the slope of the dust radiative forcing with respect to dust AOD, which is an effective method for comparison of aerosol forcing among different conditions. The resulting dust forcing efficiencies for the current test case are shown in Fig. 5a, b calculated at 380 nm and 870 nm respectively. The derived values of $f_e = -92.1$ W/m^2/AOD for wavelength 380 nm and $f_e = -94.4$ W/m^2/AOD for wavelength 870 nm, are close but higher than previous estimates of $f_e \sim -80$ W/m^2/AOD (Li et al., 2004; Yoon et al., 2005) and of $f_e \sim -69$ W/m^2/AOD (Martínez Avellaneda et al., 2010) (using ship based measurements along the coast of Africa). The variation in the findings for dust forcing efficiency also attributes due to different datasets and regional variations, for example, Li et al. (2004) used satellite observations (clouds and the earth as radiant energy system (CERES)) and the moderate resolution imaging spectroradiometer (MODIS) instruments to determine Saharan dust broadband shortwave aerosol radiative forcing over the a large part of the Atlantic Ocean near the African coast (15°25°N, 45°15°W). The findings by Yoon et al. (2005) are derived via NCAR climate model and Aeronet observations covering the Sahara region in continental Africa.

3.4. Ångström exponent and aerosol size distribution

Depending on particle size distribution, the spectral dependence of the aerosol optical depth is given approximately by Ångström (1964),

$$\frac{\tau_\lambda}{\tau_{\lambda_0}} = \left(\frac{\lambda}{\lambda_0}\right)^{-\alpha}, \tag{3}$$

where, τ_λ is the optical depth at wavelength λ, and τ_{λ_0} is the optical depth at the reference wavelength λ_0. Ångström exponent (α) can be used to estimate the dominant aerosol size based on the relation of the spectral shape of the extinction verses the particle size.

The Aeronet-retrieved Ångström exponent (Eck et al., 1999; Toledano et al., 2007) for different wavelengths is shown separately in Fig. 6(a) for 5–19 February, and Fig. 6(b) for the dust event day of February 7, 2012. Comparing the Ångström exponent distribution with the AOD values (Fig. 6(c)) confirms that the desert dust is indeed the prominent aerosol in this case with lower values of Ångström exponent (≤ 1) and corresponding high (and relatively constant) values of aerosol optical depth in various wavelength ranges (Toledano et al., 2007). In the figure, prominent values with high AOD values and low Ångström exponent indicate larger particle size of aerosols, i.e., desert dust. The few negative values of the Ångström exponent occur on account of possible cloud contamination (Toledano et al., 2007) and/or outliers due to noise in the observational data.

The aerosol particle size distribution available from the Aeronet inversion products (Dubovik & King, 2000) is shown in Fig. 7(a) for February 6 and 7, 2012. In Fig. 7(a), the volume-averaged dust aerosol concentration (effective radius approximately 2 μm) increases significantly from February 6 (dotted black line) to February 7, 2012 (colored solid lines for different times over the dust day), following the dust event. The single scattering albedo (SSA) is the ratio of the scattering to the total extinction coefficients of aerosol particles and provides important information on the scattering and absorption properties of aerosols. The corresponding SSA retrieved from Aeronet data as described by Dubovik and King (2000) for February 6 and 7, 2012, are shown in Fig. 7(b). As seen in Fig. 7(b) the spectral variability of the SSA during dusty and non-dusty days, shows that there is a large increase in the SSA on the dusty day (Feb. 7) compared with the non-dusty day (Feb. 6) for wavelengths of >600 nm. The SSA varied from 0.94 to 0.98 on the non-dusty day, and from 0.90 to 0.99 on the dusty day, with a lowest value at short wavelengths of <600 nm. The maximum SSA value of 0.99 occurred at a wavelength of 1020 nm, which is an indication of the dust aerosol (Alam, Trautmann, Blaschke, & Subhan, 2014). In agreement with other studies (Alam et al., 2014; Prasad & Singh, 2007), the changes in the diurnal SSA observed on the cloud-free dusty day (February 7, 2012) range from 0.91 to 0.99 indicating an abrupt change in concentration of dust particles over the course of the day, showing the significant presence of desert dust in the aerosol measurements (Fig. 7(b)).

4. Discussion and concluding remarks

In this study we revisited the question of how large a reduction of solar incoming radiative forcing can be caused by Saharan mineral dust outbreaks in the eastern sub-tropical Atlantic Ocean. Using a synthesis of ground-based observations of radiation and derived optical thickness of the atmosphere, we investigated the dust aerosol optical properties during a cloud-free atmosphere during a specific Saharan dust outbreak. By comparing ground-based AOD observations to ground-based time series of radiometer measurements of solar irradiance obtained at the Cape Verde atmospheric observatory, the dust forcing efficiency was estimated to be approximately $f_e = -90$ W/m^2/AOD

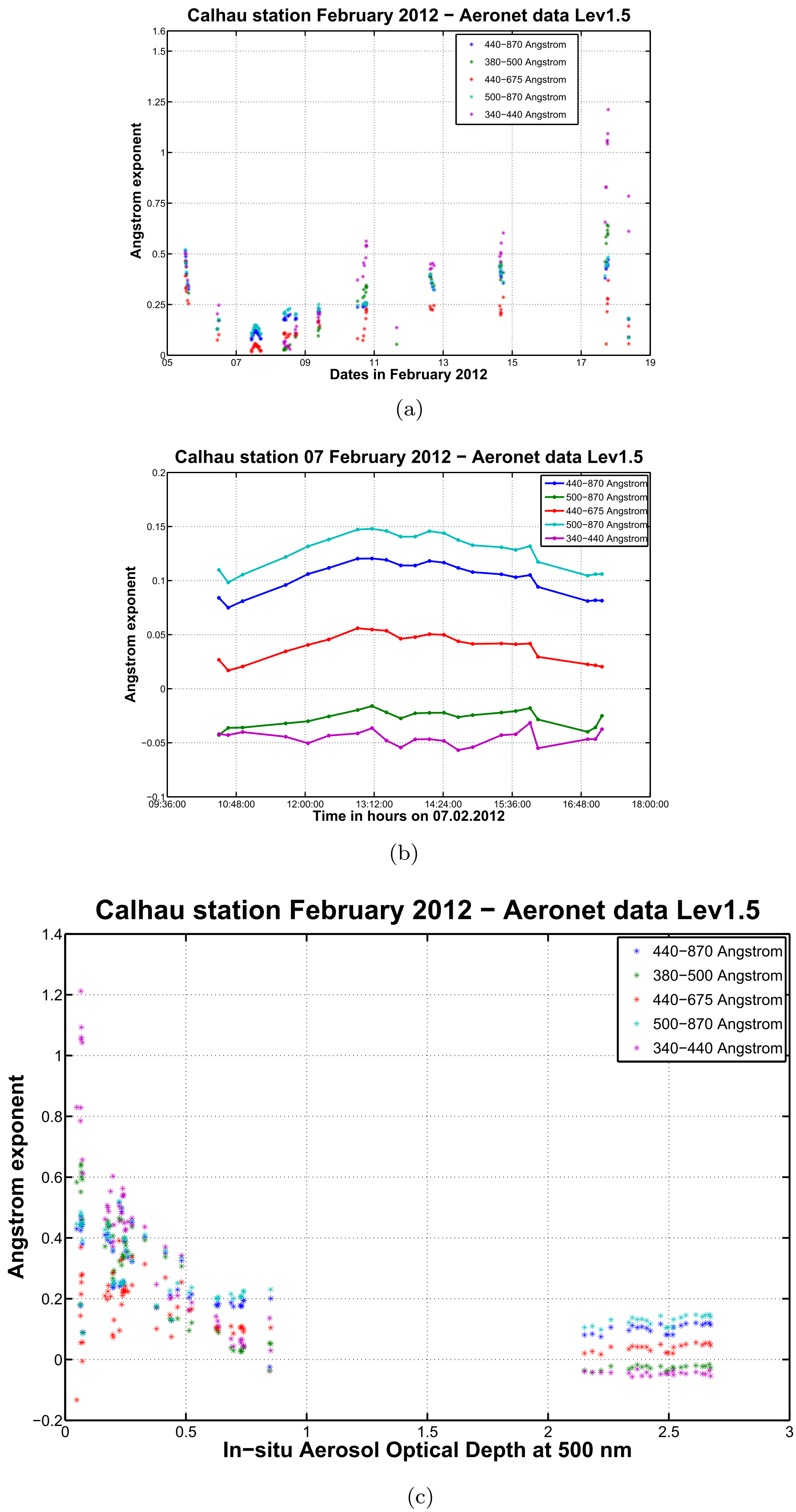

Fig. 6. (a) Aeronet-derived Ångström exponent plotted as function of wavelengths during February 6–19, 2012. (b) Ångström exponent plotted during February 7, 2012. (c) Scatter plot of Ångström exponent versus aerosol optical depth in February 2012.

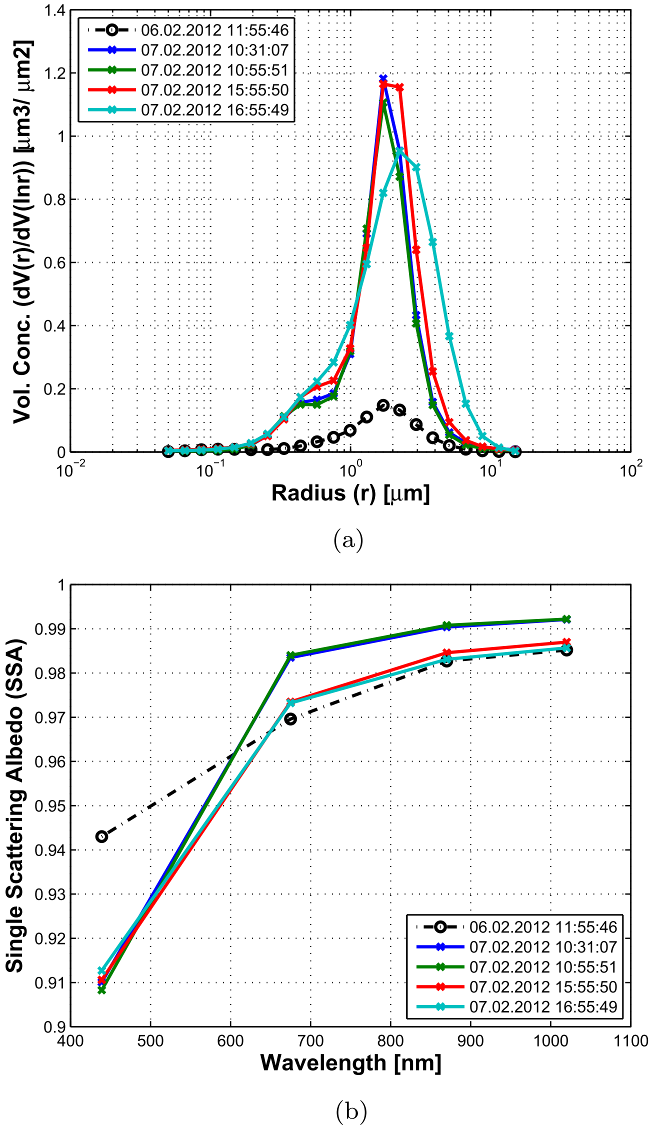

Fig. 7. (a) Aeronet derived volume concentration comparison for 6th (black dotted line) and 7th February (colored solid lines for different times) 2012 showing the significant increase in concentration of dust particles (radius approx. 2 μm) on the dust event of February 7 in comparison to the previous day; (b) Aeronet derived single scattering albedo (SSA) comparison for 6th (black dotted line) and 7th February (colored solid lines for different times) 2012.

at 380 nm, which is larger by 10–15% than values previously reported in the literature. The earlier estimates of f_e were made at lower AODs, so our result is suggestive of a dependence of f_e on AOD, perhaps caused by increased multiple scattering within a high AOD aerosol layer.

Using a cloud-free dust outbreak event during February 7, 2012, we were able to show that the derived optical thickness of the atmosphere substantially increases to above 2.5 during that day from a usual background AOD level of 0.5 or less. At the same time the derived AOD levels agree well with MODIS based AOD products and show a clear temporal AOD variability, even on a sub-daily time scale. We were able to show that, in principle, the temporal AOD changes observed during the dust outbreak event can be explained by a spatial AOD pattern that is being advected horizontally over the observatory site. Thus, the advection of spatial distributions derived from satellite imagery can be translated into temporal variations at a fixed location using a readily-available atmospheric trajectory model.

A study of the type presented here requires atmospheric conditions to be suitable, especially having cloud-free conditions. We show results from one pilot study which allowed us to investigate a strong dust event under almost perfect conditions. In the next step we aim to screen the entire time series of radiation and AOD measurements available over several months to investigate whether our findings are consistent with other similar dust outbreak events; this would allow us to derive more statistically reliable results. This will also include an investigation into the extent to which Saharan dust leads to a spectral dependence in the atmospheric attenuation spectrum.

Acknowledgments

Thanks go to the MPI in Jena, Germany for letting us use their observatory. The current work established a new Aeronet site at the Cape Verde atmospheric observatory. We thank M. Fischer for the technical assistance in site maintenance. This study was supported in part through the BMBF funded SOPRAN project (Grant 03F0611E, TP 1.5). MODIS aerosol data were provided by NASA's Giovanni portal, an online data visualization and analysis tool maintained by the Goddard Earth Sciences (GES) Data and Information Services Center (DISC), a section of the NASA Earth–Sun System Division (http://giovanni.gsfc.nasa.gov). The authors gratefully acknowledge the NOAA Air Resources Laboratory (ARL) for the provision of the HYSPLIT transport and dispersion model and the READY website (http://www.ready.noaa.gov) used in this publication. Contribution to the DFG-funded excellence initiative CliSAP of the Universität Hamburg is gratefully acknowledged.

References

Acker, J.G., & Leptoukh, G. (2007). Online analysis enhances use of NASA Earth science data. *Eos, Transactions American Geophysical Union*, *88*(2), 14–17.

Alam, K., Trautmann, T., Blaschke, T., & Subhan, F. (2014). Changes in aerosol optical properties due to dust storms in the Middle East and Southwest Asia. *Remote Sensing of Environment*, *143*, 216–227.

Albrecht, B.A. (1989). Aerosols, cloud microphysics and fractional cloudiness. *Science*, *245*, 1227–1230.

Ångström, A. (1964). The parameters of atmospheric turbidity. *Tellus*, *16*, 64–76.

Astronomical Applications Department (1990). *Astronomical Almanac*. Washington, DC and London, UK: U.S. Naval Observatory and Her Majestys Nautical Almanac Office, Royal Greenwich Observatory.

Chan, P.W. (2009). Comparison of aerosol optical depth (AOD) derived from ground-based LIDAR and MODIS. *The Open Atmospheric Science Journal*, *3*, 131–137.

Chen, Y., & Siefert, R.L. (2004). Seasonal and spatial distributions and dry deposition fluxes of atmospheric total and labile iron over the tropical and subtropical North Atlantic Ocean. *Journal of Geophysical Research: Atmospheres*, *109*, D09305http://dx.doi.org/10.1029/2003JD003958.

Chiapello, I., Bergametti, G., Chatenet, B., Bousquet, P., Dulac, F., & Soares, E.S. (1997). Origins of African dust transported over the northeastern tropical Atlantic. *Journal of Geophysical Research*, *102*(D12)http://dx.doi.org/10.1029/97JD00259.

Chiapello, I., Moulin, C., & Prospero, J.M. (2005). Understanding the long-term variability of African dust transport across the Atlantic as recorded in both Barbados surface concentrations and large-scale total ozone mapping spectrometer (TOMS) optical thickness. *Journal of Geophysical Research*, *110*, D18S10http://dx.doi.org/10.1029/2004JD005132.

Chin, M., Ginoux, P., Kinne, S., Holben, B.N., Duncan, B.N., Martin, R.V., et al. (2002). Tropospheric aerosol optical thickness from the GOCART model and comparisons with satellite and sun photometer measurements. *Journal of Atmospheric Science*, *59*, 461–483.

Draxler, R.R., & Rolph, G.D. (2013). *HYSPLIT (hybrid single-particle Lagrangian integrated trajectory) model access via NOAA ARL READY*. Website (http://www.arl.noaa.gov/HYSPLIT.php) College Park, MD: NOAA Air Resources Laboratory.

Dubovik, O., & King, M.D. (2000). A flexible inversion algorithm for retrieval of aerosol optical properties from sun and sky radiance measurements. *Journal of Geophysical Research*, *105*, 20,673–20,696.

Eck, T.F., Holben, B.N., Reid, J.S., Dubovik, O., Smirnov, A., ONeill, N.T., et al. (1999). The wavelength dependence of the optical depth of biomass burning, urban and desert dust aerosols. *Journal of Geophysical Research*, *104*, 31333–31350.

Evan, A.T., Foltz, G.R., Zhang, D., & Vimont, D.J. (2011). Influence of African dust on ocean–atmosphere variability in the tropical Atlantic. *Nature Geoscience*, *4*, 762–765.

Forster, P., Ramaswamy, V., Artaxo, P., Berntsen, T., Betts, R., Fahey, D.W., et al. (2007). Changes in atmospheric constituents and in radiative forcing. In S. Solomon, D. Qin, M. Manning, Z. Chen, M. Marquis, K.B. Averyt, M. Tignor, & H.L. Miller (Eds.), *Climate change 2007: The physical science basis. Contribution of Working Group I to the Fourth Assessment Report of the Intergovernmental Panel on Climate Change*. Cambridge, United Kingdom and New York, NY, USA: Cambridge University Press.

Holben, B.N., Eck, T.F., Slutsker, I., Tanre, D., Buis, J.P., Setzer, A., et al. (1998). AERONET — A federated instrument network and data archive for aerosol characterization. *Remote Sensing of Environment*, *66*, 1–16.

Holben, B.N., Tanre, D., Smirnov, A., Eck, T.F., Slutsker, I., Abuhassa, N., et al. (2001). An emerging ground-based aerosol climatology: Aerosol optical depth from AERONET. *Journal of Geophysical Research*, *106*, 12067–12097.

Kaufman, Y.J., Koren, I., Remer, L.A., Tanre, D., Ginoux, P., & Fan, S. (2005). Dust transport and deposition observed from the Terra-Moderate Resolution Imaging Spectroradiometer (MODIS) spacecraft over the Atlantic Ocean. *Journal of Geophysical Research*, *110*, D10S12http://dx.doi.org/10.1029/2003JD004436.

Kaufman, Y.J., Tanre, D., & Boucher, O. (2002). A satellite view of aerosols in the climate system. *Nature*, *419*, 215–223.

Kaufman, Y.J., Tanre, D., Dubovik, O., Karnieli, A., & Remer, L.A. (2001). Absorption of sunlight by dust as inferred from satellite and ground-based remote sensing. *Geophysical Research Letters*, *28*, 1479–1482.

Kirk, J.T.O. (1994). *Light and photosynthesis in aquatic ecosystems*. Cambridge: Cambridge University Press.

Lau, K.M., & Kim, K.M. (2007). Cooling of the Atlantic by Saharan dust. *Geophysical Research Letters*, *30*(12), 1655http://dx.doi.org/10.1029/2007GL031538.

Li, X., Mating, H., Savoie, D., Voss, K., & Prospero, J.M. (1996). Dominance of mineral dust in aerosol light-scattering in the North Atlantic trade winds. *Nature*, *42*(380), 416–419.

Li, F., Vogelmann, A.M., & Ramanathan, V. (2004). Saharan dust aerosol radiative forcing measured from space. *Journal of Climate*, *17*, 2558–2571.

Martínez Avellaneda, N., Serra, N., Minnett, P.J., & Stammer, D. (2010). Response of the eastern subtropical Atlantic SST to Saharan dust: A modeling and observational study. *Journal of Geophysical Research*, *115*http://dx.doi.org/10.1029/2009JC005692.

Nisantzi, A., Hadjimitsis, G.D., & Alexakis, D. (2011). Estimating the relationship between aerosol optical depth and PM10 using lidar and meteorological data in Limassol, Cyprus. *Proc. SPIE 8182, Lidar Technologies, Techniques, and Measurements for Atmospheric Remote Sensing VII, 818217*.

Pfister, G., McKenzie, R.L., Liley, J.B., Thomas, A., Forgan, B.W., & Long, C.N. (2003). Cloud coverage based on all-sky imaging and its impact on surface solar irradiance. *Journal of Applied Meteorology*, *42*, 1421–1443.

Prasad, A.K., & Singh, R.P. (2007). Changes in aerosol parameters during major dust storm events (2001–2005) over the Indo-Gangetic Plains using AERONET and MODIS data. *Journal of Geophysical Research*, *112*http://dx.doi.org/10.1029/2006JD007778.

Prospero, J.M. (1996). Saharan dust transport over the North Atlantic Ocean and Mediterranean: An overview. In S. Guerzoni, & R. Chester (Eds.), *The impact of desert dust across the Mediterranean* (pp. 133–151). Netherlands: Springer.

Prospero, J.M. (1999). Long-range transport of mineral dust in the global atmosphere: Impact of African dust on the environment of the southeastern United States. *Proceedings of the National Academy of Sciences of the United States of America*, *96*, 3396–3403.

Prospero, J.M., & Carlson, T.N. (1972). Indian Ocean experiment: Vertical and areal distribution of Saharan dust over the western Equatorial North Atlantic Ocean. *Journal of Geophysical Research*, *77*, 5255–5265.

Ramanathan, V., et al. (2001). Indian Ocean experiment: An integrated analysis of the climate forcing and effects of the great Indo-Asian haze. *Journal of Geophysical Research*, *106*(D22)http://dx.doi.org/10.1029/2001JD900133.

Rosenfeld, D., Rudich, Y., & Lahav, R. (2001). Desert dust suppressing precipitation: A possible desertification feedback loop. *Proceedings of the National Academy of Sciences of the United States of America*, *98*http://dx.doi.org/10.1073/pnas.101122798.

Schütz, L. (1980). Long range transport of desert dust with special emphasis on the Sahara. *Annals of the New York Academy of Sciences*, *338*, 515–532.

Smirnov, A., Holben, B.N., Eck, T.F., Dubovik, O., & Slutsker, I. (2000). Cloud-screening and quality control algorithms for the AERONET database. *Remote Sensing of Environment*, *73*(3), 337–349.

Smirnov, A., Holben, B.N., Eck, T.F., Slutsker, I., Chatenet, B., & Pinker, R.T. (2002). Diurnal variability of aerosol optical depth observed at AERONET (Aerosol Robotic Network) sites. *Geophysical Research Letters*, *29*http://dx.doi.org/10.1029/2002GL016305.

Sokolik, I.N., Winker, D.M., Bergametti, G., Gillette, D.A., Carmichael, G., Kaufman, Y.J., et al. (2001). Introduction to special section: Outstanding problems in quantifying the radiative impacts of mineral dust. *Journal of Geophysical Research*, *106*(D16), 18,015–18,027.

Stocker, T.F., Qin, D., Plattner, G. -K., Tignor, M., Allen, S.K., & Boschung, J., et al. (Eds.). (2013). *Climate Change 2013: The physical science basis. Contribution of Working Group I to the Fifth Assessment Report of the Intergovernmental Panel on Climate Change*. Cambridge, United Kingdom and New York, NY, USA: Cambridge University Press.

Tegen, I., Hollrig, P., Chin, M., Fung, I., Jacob, D.J., & Penner, J. (1997). Contribution of different aerosol species to the global aerosol extinction optical thickness: Estimates from model results. *Journal of Geophysical Research*, *102*http://dx.doi.org/10.1029/97JD01864.

Thuillier, G., Hersé, M., Simon, P.C., Labs, D., Mandel, H., Gillotay, D., et al. (2003). The solar spectral irradiance from 200 to 2400 nm as measured by the SOLSPEC spectrometer from the ATLAS 1–2–3 and EURECA missions. *Solar Physics*, *214*(1), 1–22.

Toledano, C., Cachorro, V.E., Berjon, A., de Frutos, A.M., Sorribas, M., de la Morena, B.A., et al. (2007). Aerosol optical depth and Ångström exponent climatology at El Arenosillo AERONET site (Huelva, Spain). *Quarterly Journal of the Royal Meteorological Society*, *133*, 795–807http://dx.doi.org/10.1002/qj.5.

Twomey, S.A. (1977). The influence of pollution on the shortwave albedo of clouds. *Journal of Atmospheric Science*, *34*, 1149–1152.

Vogelmann, A.M., Flatau, P.J., Szczodrak, M., Markowicz, K., & Minnett, P.J. (2003). Observations of large aerosol infrared forcing at the surface. *Geophysical Research Letters*, *30*, 1655.

Winker, D.M., Pelon, J., & McCormick, M.P. (2002). The CALIPSO Mission: Spaceborne lidar for observation of aerosols and clouds. *Proceedings of SPIE*, *4893*, 1–11.

Yoon, S.C., Won, J.G., Omar, A.H., Kim, S.W., & Sohn, B. -J. (2005). Estimation of the radiative forcing by key aerosol types in worldwide locations using a column model and AERONET data. *Atmospheric Environment*, *39*, 6620–6630.

Zhu, A., Ramanathan, V., Li, F., & Kim, D. (2007). Dust plumes over the Pacific, Indian, and Atlantic oceans: Climatology and radiative impact. *Journal of Geophysical Research*, *112*http://dx.doi.org/10.1029/2007JD008427.